High-Temperature Shock Tube Studies Using Multipass Absorption: Rate Constant Results for OH + CH_3, OH + CH_2, and the Dissociation of CH_3OH

L. N. Krasnoperov[‡] and J. V. Michael*[,§]

Department of Chemistry and Environmental Science, New Jersey Institute of Technology, University Heights, Newark, New Jersey 07102 and Chemistry Division, Argonne National Laboratory, Argonne, Illinois 60439

Received: May 7, 2004; In Final Form: July 6, 2004

The reflected shock tube technique with multipass absorption spectrometric detection has been used to study the reactions of OH radicals: (1) OH + $CH_3 \rightarrow {}^1CH_2 + H_2O$, (2) OH + $^3CH_2 \rightarrow CH_2O + H$, and the thermal dissociation of methanol, (3) $CH_3OH \rightarrow CH_3 + OH$. (1) has never been studied above 1000 K, (2) has never been studied, and (3) has been studied but with conflicting results. Depending on conditions, all three reactions can be important in combustion systems, and this realization supplies the motivation for the present study. *tert*-Butyl hydroperoxide, di-*tert*-butyl peroxide, methanol, and methyl iodide were used as pyrolytic precursors of hydroxyl and methyl radicals. Methylene was produced by the pyrolysis of ketene. The experiments were performed in single-shot experiments with low initial concentrations of hydroxyl radicals, $[OH]_0 = (4.5-130) \times 10^{12}$ molecules cm^{-3}. $[OH]_t$ was measured with resonance absorption around 308 nm. The measured rate constants are $k_1 = 1.74 \times 10^{-11} \exp(915\ K/T)$ (834−2383 K), $k_2 = (2.6 \pm 1.6) \times 10^{-11}$ (1841−2324 K), and $k_3 = 4.39 \times 10^{-8} \exp(-31\,938\ K/T)$, all in cm^3 $molecule^{-1}$ s^{-1}. In addition, the yield of OH radicals in the pyrolysis of methanol was determined, 0.94 ± 0.09 (1841−2309 K). Where possible, these results are compared to earlier data and estimates. Existing theory is also reviewed and compared to the present results.

Introduction

Due to their importance in combustion chemistry, the rate constants for

$$OH + CH_3 \rightarrow \text{products} \qquad (1)$$

and

$$OH + CH_2 \rightarrow \text{products} \qquad (2)$$

have been the subject of considerable earlier study.[1−3] These radical recombinations are nearly barrierless. At lower temperatures, both reactions are therefore chemical activation cases from vibrationally excited methanol and hydroxy-methyl radicals, respectively. Five forward decomposition channels for reaction 1 have already been discussed in detail by De A. Pereira et al.[2] and Xia et al.,[3] and the zero-point corrected values for $\Delta H_0°$ in kcal mol^{-1} for each reaction are taken from Xia et al.[3]

$$OH + CH_3 \rightarrow CH_3OH \quad (-91.9) \qquad (1a)$$

$$\rightarrow {}^1CH_2 + H_2O \quad (-1.6) \qquad (1b)$$

$$\rightarrow CH_3O + H \quad (+13.0) \qquad (1c)$$

$$\rightarrow CH_2OH + H \quad (+4.3) \qquad (1d)$$

$$\rightarrow CH_2O + H_2 \quad (-73.8) \qquad (1e)$$

$$\rightarrow \textit{cis-,trans-}\ HCOH + H_2 \quad (-17.4 \text{ and } -21.4) \qquad (1f)$$

In addition, the channel on the triplet potential energy surface should be considered at elevated temperatures:[4]

$$OH + CH_3 \rightarrow {}^3CH_2 + H_2O \quad (-11.2) \qquad (1g)$$

The only products energetically possible from reaction 2 are apparently $CH_2O + H$.[1]

The thermal decomposition of methanol,

$$CH_3OH \rightarrow CH_3 + OH \qquad (3)$$

is a convenient source for simultaneous generation of hydroxyl and methyl radicals. This reaction has also been extensively studied.[1,3,5]

In the present work, a multipass absorption technique has been used at 308 nm to monitor OH-radical concentrations in reflected shock tube experiments.[6] Rate constants have been measured for reactions 1−3, and the present results are compared to earlier data and theory.

Experimental Section

The present experiments were performed with the reflected shock tube technique using OH-radical electronic absorption detection. The method and the apparatus currently being used have been previously described,[6−8] and only a brief description of the experiment will be presented here.

The apparatus consists of a 7-m (4-in. o.d.) 304 stainless steel tube separated from the He driver chamber by a 4-mil unscored 1100-H18 aluminum diaphragm. The tube was routinely pumped between experiments to $<10^{-8}$ Torr by an Edwards Vacuum Products Model CR100P packaged pumping system. The velocity of the shock wave was measured with eight equally spaced pressure transducers (PCB Piezotronics, Inc., Model 113A21) mounted along the end portion of the shock tube, and

* Corresponding Author: Dr. J. V. Michael D-193, Bldg. 200 Argonne National Laboratory Argonne, Illinois 60439. Phone: (630) 252-3171. Fax: (630) 252-4470. E-mail: jmichael@anl.gov.
‡ New Jersey Institute of Technology.
§ Argonne National Laboratory.

10.1021/jp040343+ CCC: $27.50
Published on Web 09/14/2004

temperature and density in the reflected shock wave regime were calculated from this velocity and include corrections for boundary layer perturbations.[9−11] A 4094C Nicolet digital oscilloscope was used to record velocity gauge signals, and an LC334A LeCroy digital oscilloscope was used to record the absorption signals. Delayed pulses that derive from the last velocity gauge signal triggered both scopes.

In these experiments we used an OH resonance lamp as described previously.[6,12,13] A detailed description of the absorption cell and the theory of operation are given elsewhere.[6,14] The effective gain in this multipass cell was checked using absorption of the monitoring light by a stable compound, acetone. The cross-section of acetone was measured in a single-pass arrangement: σ(acetone, 296 K) = (1.492 ± 0.022) × 10^{-20} cm^2 molecule^{-1} for the MW discharge OH resonance lamp around 308 nm. The cell calibration and gain stability were routinely measured, giving the effective cell gain as G = (11.0 ± 1.0).

Reflected shock tube experiments were then performed, and the details of the lamp operating conditions as well as of the OH absorption cross-section measurements are described earlier.[6] The effective OH-radical absorption coefficient for the multi-line light from the lamp was determined to be σ_{OH} = (4.16−1.05 × 10^{-3} T) × 10^{-17} cm^2 molecule^{-1} over the temperature range, 1116−1875 K. This compares well with previous studies[12,13] where a multiline source of OH radiation has also been used.

Gases. High-purity He (99.995%), used as the driver gas, was from AGA Gases. Scientific-grade Kr (99.999%), the diluent gas in reactant mixtures, was from Spectra Gases, Inc. The ~10 ppm impurities (N_2: 2 ppm; O_2: 0.5 ppm; Ar: 2 ppm; CO_2: 0.5 ppm; H_2: 0.5 ppm; CH_4: 0.5 ppm; H_2O: 0.5 ppm; Xe: 5 ppm; and CF_4: 0.5 ppm) are all either inert or in sufficiently low concentration so as to not perturb OH-radical profiles. Distilled water, evaporated at one atmosphere into ultrahigh purity grade Ar (99.999%) from AGA Gases, was used at ~25 Torr pressure in the resonance lamp. The CH_3I (99%), obtained from Aldrich Chemical Co. Inc, and CH_3OH (99.8%), obtained from Sigma Aldrich Chemical Co., were further purified by bulb-to-bulb distillation with the middle thirds being retained for mixture preparation. The 98% *di*-tertiary butyl peroxide (*di-tert*-butyl P) and 90% tertiary butyl hydroperoxide (*tert*-butyl HP) were both obtained from Sigma Aldrich Chemical Co. and were used as received. The latter compound is unstable; therefore, an NMR analysis was carried out giving an actual purity level of 71%. Ketene was prepared from the pyrolysis of acetic anhydride and was bulb-to-bulb distilled, retaining only the middle third. Test gas mixtures were accurately prepared from pressure measurements using a Baratron capacitance manometer and were stored in an all glass vacuum line.

Results and Discussion

Reaction OH + CH_3. OH-radical absorption experiments have been carried out to determine k_1. In the lower temperature regime (i.e., 800−1350 K), OH and CH_3 radicals were simultaneously prepared from the thermal decomposition of *tert*-butyl hydroperoxide, $(CH_3)_3COOH$

$$(CH_3)_3COOH \rightarrow (CH_3)_3CO + OH \rightarrow (CH_3)_2CO + CH_3 + OH \quad (4)$$

tert-Butyl hydroperoxide has been used previously[15] for OH preparation. In the present experiments, equal quantities of both OH and CH_3 are formed almost instantaneously in reaction 4. To increase the effect of reaction 1 relative to the radical self-reactions, we added excess *di-tert*-butyl peroxide to the reaction mixture as an additional CH_3-radical producer, thereby varying the ratio of the initial concentrations of the two radicals, $[CH_3]_0/[OH]_0$. This molecule also decomposes almost instantaneously in two steps

$$(CH_3)_3COO(CH_3)_3 \rightarrow 2(CH_3)_3CO \rightarrow 2(CH_3)_2CO + 2CH_3 \quad (5)$$

to give excess $[CH_3]_0$. Hydroxyl and methyl radicals formed in reactions 4 and 5 are subsequently depleted mainly in reaction 1, in CH_3-radical recombination,[16] and in the OH-radical self-reaction,[17]

$$OH + OH \rightarrow H_2O + O \quad (6)$$

Several minor additional reactions of these radicals and other secondary reactions were added to fit the experimental profiles. A complete list of the chemical mechanism is included in the Supporting Information. Nonlinear mean square fits by numerical solutions of the differential equations describing the mechanism were used for data processing. In these fits, k_1 was used as the unknown fitting parameter.

Three single-pass absorption experiments using the pyrolysis of *tert*-butyl hydroperoxide alone have been carried out and are listed in Table 1 along with the values for k_1. Under single-pass conditions the lifetime of the radicals is short both due to self-reactions and the cross-radical−radical reaction between OH and CH_3. One multipass experiment was then carried out at substantially lower $[OH]_0$ and $[CH_3]_0$, thereby increasing the depletion time. The result for k_1 is also listed in Table 1. Thirteen additional experiments were then performed with *tert*-butyl hydroperoxide and *di-tert*-butyl peroxide mixtures using multipass detection. These experiments were also analyzed, and the conditions and results are also given in Table 1.

To study the reaction at higher temperatures, we used the thermal decomposition of CH_3OH as a source for both $[OH]_0$ and $[CH_3]_0$:

$$CH_3OH \rightarrow CH_3 + OH \quad (3a)$$

$$\rightarrow \text{other products} \quad (3b-3f)$$

In seven experiments, we increased $[CH_3]_0$ by simultaneously decomposing known concentrations of added CH_3I. As with the *tert*-butyl hydroperoxide/*di-tert*-butyl peroxide experiments, the OH experimental profiles were likewise simulated using the reaction mechanism (Supporing Information). Again, the mechanism consisted of reaction 1, OH and CH_3 radical self-reactions, and additional reactions of minor importance. An example of an OH absorption profile together with the fitted curve and other simulations is shown in Figure 1. It is apparent that reaction 1 gives the major contribution to the OH decay under the current experimental conditions. The second most important reaction is the self-reaction of OH radicals. The other reactions included in the mechanism play only a very minor role. However, in experiments with water addition where both reactions 1b and 6 are completely repressed by shifting the equilibrium toward the reactants, the residual reactions in the mechanism become important (see below).

In the CH_3OH thermal decomposition experiments at somewhat lower temperatures than shown in Figure 1, both the buildup and the decay of OH radicals could be time resolved. This allowed simultaneous determination of both rate constants for CH_3OH decomposition (reaction 3) and OH + CH_3 (reaction

TABLE 1: Rate Data for OH + CH_3 → CH_2 + H_2O and CH_3OH → CH_3 + OH

P_1/Torr	M_s[a]	$\rho_5/(10^{18}$ cm$^{-3})$[b,c]	T_5/K[b]	k_1[d]	k_3[d]
		$X_{tert\text{-butyl HP}} = 7.761 \times 10^{-5}$[c]			
10.87[e]	2.114	1.727	1155	3.85(−11)[f]	
10.86[e]	2.002	1.607	1048	4.39(−11)	
10.88[e]	1.797	1.377	867	6.05(−11)	
		$X_{tert\text{-butyl HP}} = 7.703 \times 10^{-6}$			
10.89	2.079	1.694	1121	5.41(−11)	
$X_{tert\text{-butyl HP}} = 7.630 \times 10^{-6}$			$X_{di\text{-}tert\text{-butyl P}} = 7.499 \times 10^{-6}$		
5.93	1.948	0.845	999	3.61(−11)	
5.94	2.064	0.915	1107	2.95(−11)	
10.98	1.765	1.359	834	3.66(−11)	
10.96	2.016	1.643	1058	3.58(−11)	
10.90	1.856	1.453	914	3.93(−11)	
10.91	1.924	1.533	974	3.89(−11)	
10.89	2.139	1.762	1176	5.03(−11)	
10.98	2.040	1.672	1080	3.98(−11)	
10.89	1.881	1.481	935	4.71(−11)	
20.89	1.855	2.750	906	6.34(−11)	
20.98	1.805	2.651	864	4.96(−11)	
20.89	2.056	3.163	1084	4.86(−11)	
20.90	2.045	3.142	1073	6.22(−11)	
		$X_{CH_3OH} = 5.693 \times 10^{-6}$			
10.94	2.705	2.247	1817	2.01(−11)	1.71(−15)
10.90	2.928	2.389	2104	1.47(−11)	8.04(−15)
10.88	2.980	2.416	2175	3.75(−11)	1.92(−14)
10.94	3.104	2.502	2348	3.56(−11)	6.00(−14)
10.90	3.129	2.507	2383	2.52(−11)	5.98(−14)
20.86	3.108	4.625	2304	3.76(−11)	3.24(−14)
20.79	2.935	4.430	2072	3.27(−11)	5.26(−15)
20.85	2.952	4.462	2094	1.91(−11)	7.44(−15)
20.86	2.857	4.357	1972	2.29(−11)	2.39(−15)
		$X_{CH_3OH} = 1.080 \times 10^{-5}$			
10.94	2.944	2.408	2126	2.95(−11)	
10.92	2.925	2.391	2100	2.95(−11)	
10.91	2.892	2.368	2057	3.52(−11)	
10.92	2.904	2.378	2072	2.26(−11)	
20.90	2.971	4.509	2112	2.99(−11)	
$X_{CH_3OH} = 6.015 \times 10^{-6}$			$X_{CH_3I} = 9.950 \times 10^{-6}$		
10.94	2.927	2.397	2103	2.22(−11)	1.50(−14)
10.88	2.992	2.432	2185	2.77(−11)	1.50(−14)
10.93	3.108	2.511	2346	3.47(−11)	5.97(−14)
10.87	2.765	2.283	1886	2.31(−11)	1.57(−15)
10.83	2.995	2.423	2188	3.12(−11)	6.19(−14)
20.90	3.099	4.641	2284	2.36(−11)	3.23(−14)
20.83	2.971	4.494	2112	2.11(−11)	2.04(−14)

[a] Error in measuring the Mach number, M_s, is typically 0.5−1.0% at the one standard deviation level. [b] Quantities with the subscript 5 refer to the thermodynamic state of the gas in the reflected shock region. [c] ρ refers to the total density in the reflected shock tube regime, and X_i refers to the mole fraction of species i in the mixture. [d] Rate constants in units cm^3 molecule^{-1} s^{-1}. [e] Denotes single-pass experiments, all others are multipass experiments. [f] Parentheses denotes the power of 10.

1) by fitting the entire concentration profile. Since the characteristic times for OH buildup and decay differ significantly, the fitted rate constants have only a minor mutual dependence. In addition to rate constants for reactions 1 and 3, the branching ratio for (3), α_{3a}, was used as a fitting parameter. The values obtained with added CH_3I to increase $[CH_3]_0$ are also listed in Table 1. Without question, the OH-radical profiles for all the experiments in the table are strongly dominated by reaction 1; therefore, the values given can be viewed as being direct.

The values of k_1 are plotted in Arrhenius form in Figure 2. There are several room-temperature determinations of rate constants for (1)[2,18−23] ranging from ∼7 to 17 × 10^{-11} cm^3 molecule^{-1} s^{-1} for pressures in the range ∼50−940 Torr. The only study at high temperature is that of Bott and Cohen,[24] who

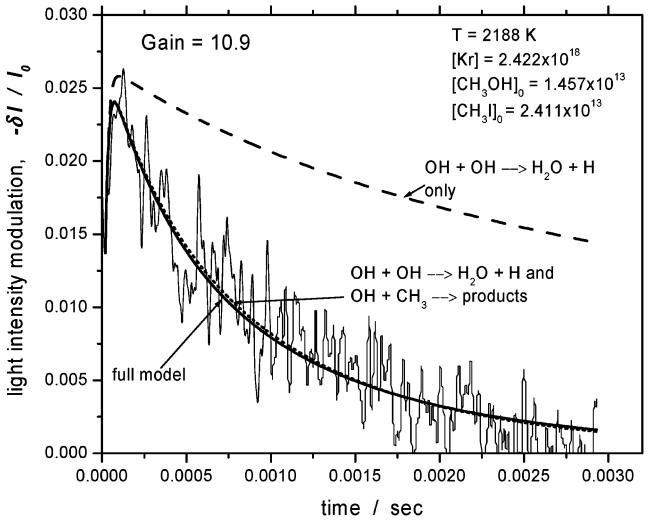

Figure 1. Sample temporal profile of OH absorption. Solid line: fit with the full reaction mechanism. Dashed line: simulation with only the OH + OH reaction in the mechanism. Dotted line: only OH + OH and OH + CH_3 reactions are taken into account. [Kr] = 2.422 × 10^{18}, $[CH_3OH]_0$ = 1.457 × 10^{13}, $[CH_3I]_0$ = 2.411 × 10^{13} molecule cm^{-3}, and T = 2188 K.

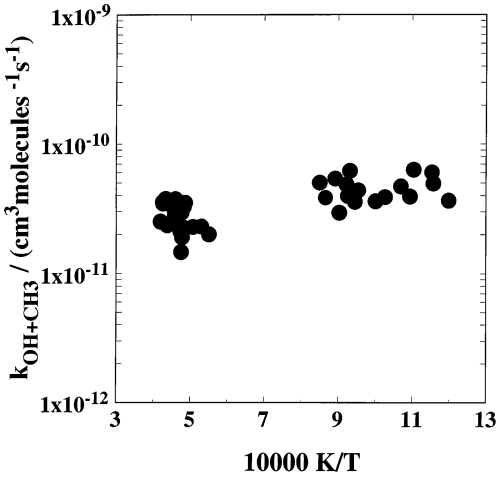

Figure 2. Arrhenius plot of the OH + CH_3 data in Table 1.

report $k_1 = (1.8 \pm 0.5) \times 10^{-11}$ cm^3 molecule^{-1} s^{-1} at 1200 K and 760 Torr Ar. This value disagrees with the present determination, being about one-third of the values shown in Table 1. A linear least-squares analysis of the Table 1 data gives the Arrhenius expression:

$$k_1 = 1.74 \times 10^{-11} \exp(915\ \mathrm{K}/T) \qquad \text{(E1)}$$

The data in Table 1 are also plotted in Figure 3 along with data in the range ∼100−700 Torr from De A. Pereira et al.[2] Using ab initio electronic structure calculations, both De A. Pereira et al.[2] and Xia et al.[3] have applied RRKM theory to estimate the importance of the channels, 1a to 1f. The absence of pressure dependence suggests that the specific forward dissociation rate constants are much faster than back dissociation to CH_3 + OH, and both RRKM theoretical studies agree with this conclusion. Theory also indicates that the only important channels are reactions 1a, 1b, and 1f. The branching ratios between these channels are strongly dependent on both temperature and pressure. For example at high pressures (P > ∼10^6 Torr), reaction 1a always dominates at any T, but at pressures of ∼1atm, the forward dissociations, reactions 1b and 1f, become

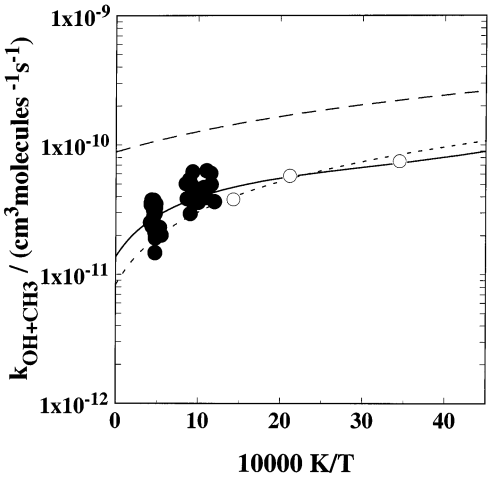

Figure 3. Arrhenius plot of the OH + CH_3 data in Table 1 (reaction l) and data from De A. Pereira et al.[2] (○) at pressures between 100 and 700 Torr. The solid line is calculated from equation E2. The short dashes are the high-pressure limit from De A. Pereira et al.[2], and the long dashes are the high-pressure limit from Xia et al.[3]

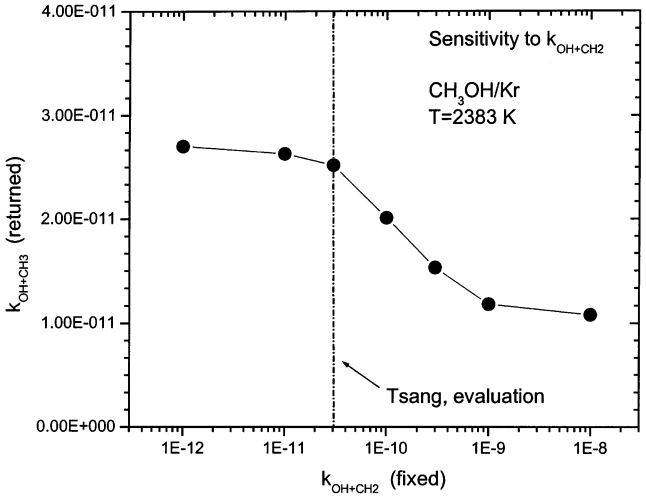

Figure 4. Sensitivity for the determination of k_1 to the rate constant for the OH + CH_2 reaction in the pyrolysis of CH_3OH/Kr with [Kr] = 2.507×10^{18}, $[CH_3OH]_0 = 1.427 \times 10^{13}$ molecule cm^{-3}, and T = 2383 K. Dotted line: Tsang's evaluation (confirmed in this work).

increasingly important as T increases. Both studies also agree that the forward dissociation, reaction 1f, accounts for only 1−2% to the reaction rate. Hence, the only important processes are stabilization, reaction 1a, and forward dissociation to $^1CH_2$ + H_2O, 1b. At ∼1 atm, the RRKM formulations predict a branching ratio of 0.5 each for reactions 1a and 1b at ∼700 K[2] and at ∼570 K,[3] respectively. With increasing T and pressures < 1 atm, stabilization (reaction 1a) becomes much less important; therefore, the only important process above ∼1000 K should be reaction 1b and should be equal to the high-pressure limit. Xia et al.[3] have calculated values for the high-pressure limit of 28×10^{-11} to 14×10^{-11} cm^3 $molecule^{-1}$ s^{-1} for temperatures of 200 to 700 K, respectively, and these are also shown in Figure 3 as the upper dashed line. On the other hand, De A. Pereira et al.[2] report a somewhat lower value of 7.245×10^{-9} $T^{-0.79}$ cm^3 $molecule^{-1}$ s^{-1} for their experimental T-range, 290−700 K. This expression is also plotted in Figure 3 as the line of short dashes. Inspection of Figure 3 shows that the present values agree better with the results of De A. Pereira et al.[2] than with the inferences from Xia et al.[3] Giving the De A. Pereira et al. results a statistical weight of 10 compared to the values from Table 1, a least-squares expression can be derived for the rate behavior for reaction 1 over the T-range, 290−2400 K, and the P-range, 100−1000 Torr,

$$k_1 = 1.15 \times 10^{-9}\, T^{-0.4884} \qquad \text{(E2)}$$

and equation E2 is plotted in Figure 3 as the solid line. Inspection of the figure shows that the rate behavior in the ∼2000 K range is a factor of 1.56 higher that the values indicated by De A. Pereira et al.[2] One possible explanation for this apparent discrepancy is that the direct abstraction reaction on the triplet potential energy surface

$$OH + CH_3 \rightarrow {}^3CH_2 + H_2O \qquad \text{(1g)}$$

may contribute above 2000 K. Using theoretical arguments, Xia et al.[3] and Wilson and Balint-Kurti[4] have proposed respective rate constant expressions:

$$k_{1g} = 2.0 \times 10^{-22}\, T^{3.39} \exp(-1412\ K/T) \qquad \text{(E3)}$$

and

$$k_{1g} = 1.85 \times 10^{-21}\, T^{3} \exp(-1400\ K/T) \qquad \text{(E4)}$$

In the 2000−2400 K range, equation E3 is about two times larger than equation E4. The former equation gives values that are too high, but the latter equation gives values that can explain the 60% discrepancy.

According to De A. Pereira et al.[2] as already mentioned, reaction 1b is the major reaction channel. The $^1CH_2$ formed in this channel is quenched on a much shorter time scale than that of the current experiments. In the mechanism used to process our experimental data, it was assumed that $^1CH_2$ and $^3CH_2$ are in thermal equilibrium. The methylene formed in reaction 1 represents a potential problem for the interpretation of the experimental OH profiles if it can react with the OH radical in reaction 2. If reaction 2 is very much faster than reaction 1, then two OH radicals are consumed, doubling the decay rate. Figure 4 shows the impact of k_2 used in the mechanism on the values of k_1 returned by the fits for a sample experimental OH profile. There are no experimental data in the literature on reaction 2. Therefore, in the initial fits the value of $k_2 = 3 \times 10^{-11}$ cm^3 $molecule^{-1}$ s^{-1} recommended by Tsang and Hampson[25] was used. It is apparent from Figure 4 that if the actual rate constant is equal to or lower than this recommended value, then reaction 2 has only a minor impact on k_1. However, if reaction 2 is much faster, then it can lower rate constants for reaction 1 almost by a factor of 2. Therefore, a limited study on the rate constant of reaction 2 was performed.

Reaction OH + CH_2. To evaluate rate constants for reaction 2, ketene (CH_2CO) was added to the gas mixture. CH_2CO dissociates rapidly at high temperatures giving $^3CH_2$ + CO:[26]

$$CH_2CO \rightarrow CH_2 + CO \qquad (7)$$

As shown in Table 2, two series of measurements were made using different reactant ratios in each set. We carried out 14 experiments over the T-range 1887−2324 K, but the experiments > 2170 K were too difficult to interpret. This was due no doubt to increasing complications from secondary reactions. The measured profiles for eight of these experiments (Table 2) could be simulated, giving values for $^3CH_2$ + OH → CH_2O + H that randomly range between (1.0−5.7) × 10^{-11} cm^3 $molecule^{-1}$ s^{-1} over the T-range 1887−2164 K and yielding k_2 = (2.6 ±

TABLE 2: Rate Data for OH + CH_2 → CH_2O + H

P_1/Torr	M_s[a]	$\rho_5/(10^{18}$ cm$^{-3})$[b,c]	T_5/K[b]	k_2[d]
$X_{CH_3OH} = 1.368 \times 10^{-5}$[c]			$X_{CH_2CO} = 2.023 \times 10^{-5}$	
10.99	2.879	2.337	2038	1.10(−11)[e]
10.93	2.925	2.393	2099	1.44(−11)
10.86	2.978	2.419	2164	3.10(−11)
20.89	2.930	4.447	2065	5.71(−11)
20.87	2.816	4.327	1914	0.97(−11)
20.87	2.933	4.446	2069	3.12(−11)
$X_{CH_3OH} = 1.065 \times 10^{-5}$			$X_{CH_2CO} = 9.968 \times 10^{-5}$	
20.95	2.796	4.305	1894	3.29(−11)
10.94	2.767	2.300	1887	2.32(−11)

[a] Error in measuring the Mach number, M_s, is typically 0.5−1.0% at the one standard deviation level. [b] Quantities with the subscript 5 refer to the thermodynamic state of the gas in the reflected shock region. [c] ρ refers to the total density in the reflected shock tube regime, and X_i refers to the mole fraction of species i in the mixture. [d] Rate constants in units cm^3 molecule^{-1} s^{-1}. [e] Parentheses denotes the power of 10.

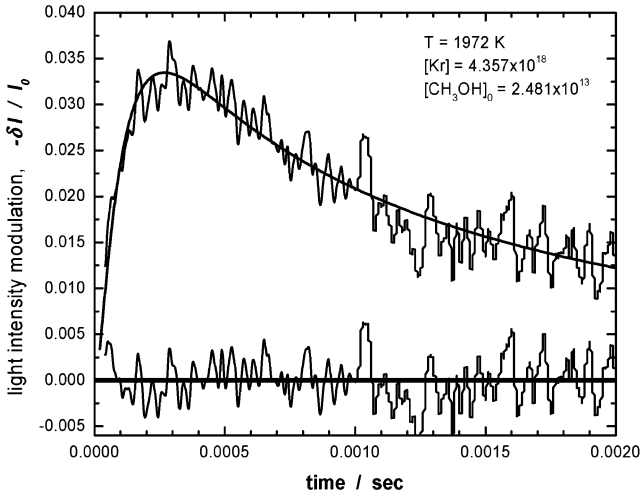

Figure 5. Typical OH profile for the decomposition of CH_3OH. Both build-up, due to decomposition, and decay, due to radical−radical reactions, are resolved at $T = 1972$ K. CH_3OH/Kr mixture with [Kr] $= 4.357 \times 10^{18}$ and $[CH_3OH]_0 = 2.481 \times 10^{13}$ molecule cm^{-3}.

1.6) $\times 10^{-11}$ cm^3 molecule^{-1} s^{-1}. The reason for the scatter in these values is not clear; however, the signal-to-noise ratio was low, and the fits required using our values for equation 1 that also occurs at a similar rate. Hence, both processes are competitive for OH-radicals.

The recommended value for k_2 from Tsang and Hampson[25] is 3×10^{-11} cm^3 molecule^{-1} s^{-1} for $300 \le T \le 2500$ K, but this evaluation is highly uncertain. The value obtained here appears to be the first relatively direct determination and corroborates the evaluation. Incorporation of this rate constant into the mechanism shows that $^3CH_2$ + OH has a minor effect on the values obtained for reaction 1 (CH_3 + OH) as shown in Figure 4. It should be noted that these determinations of k_2 are slightly correlated with the rate constants for reaction 1. The value 2.6×10^{-11} cm^3 molecule^{-1} s^{-1} was determined with the k_1 measured in this study. A somewhat higher value for k_2 $\sim 5 \times 10^{-11}$ cm^3 molecule^{-1} s^{-1} is obtained if the extrapolated value from De A. Pereira et al.[2] (i.e., 1.56 lower than the present value) is used in the data fits. However, this slightly higher value, 5×10^{-11}, has only a minor impact (<9%) on the rate constant of reaction 1 returned by the fits (Figure 4).

Dissociation of CH_3OH. As stated earlier, values for k_3 could be determined from buildup profiles in the methanol decomposition experiments, and Figure 5 shows a typical example of a profile fit where buildup and decay are time resolved. The

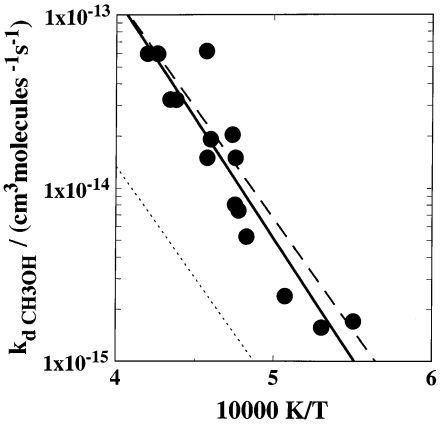

Figure 6. Arrhenius plot of bimolecular rate constants for CH_3OH dissociation. The solid line is the linear regression given in equation E5, the long dashes are equation E6, and the short dashes are from Xia et al.[3]

resultant values of k_3 are listed in Table 1 for those experiments where time resolution was possible. The present results for the thermal decomposition of CH_3OH are plotted in Figure 6 and can be described by the linear least-squares Arrhenius expression (solid line) as

$$k_3 = 4.39 \times 10^{-8} \exp(-31938\ K/T) \qquad \text{(E5)}$$

in units of cm^3 molecule^{-1} s^{-1} since this reaction is near the low-pressure second-order limit. This decomposition has been studied a number of times[1] with the most recent experimental study being that of Cribb et al.[5] who report the second-order rate constants between 1900 and 2700 K as

$$k_3 = 1.23 \times 10^{22}\ T^{-8.00} \exp(-45301\ K/T) \qquad \text{(E6)}$$

in units of cm^3 molecule^{-1} s^{-1}. The values from equation E6 are plotted as the line of long dashes and are compared to equation E5 in Figure 6. The agreement is excellent with the maximum deviation being < 33%. Most other studies agree, within experimental error, with rate constants calculated from equation E6, particularly the evaluation by Baulch et al.[27]

Even though there is generally good agreement on the overall second-order rate constants for CH_3OH decomposition, there are at least six possible channels for decomposition.

$$CH_3OH \rightarrow CH_3 + OH \qquad \text{(3a)}$$

$$\rightarrow {}^1CH_2 + H_2O \qquad \text{(3b)}$$

$$\rightarrow CH_2OH/CH_3O + H \qquad \text{(3c)}$$

$$\rightarrow CH_2O + H_2 \qquad \text{(3d)}$$

$$\rightarrow cis\text{-}HCOH + H_2 \qquad \text{(3e)}$$

$$\rightarrow trans\text{-}HCOH + H_2 \qquad \text{(3f)}$$

These have been discussed in detail by Xia et al.,[3] who suggest, on the basis of moderate level electronic structure calculations coupled to RRKM calculations, that the process giving $^1CH_2$ + H_2O is dominant at pressures < 1 atm. These authors have estimated the overall second-order rate constants at 1 atm; their values are also plotted in Figure 6 as the line of short dashes. Their theory underestimates the experimental results by about a factor of 10. Over the T-range 1700−2500 K, these authors[3] have also theoretically predicted branching ratios for reactions 3a−3f, reporting 0.33, 0.52, 0, 0, 0.13, and 0.01, respectively,

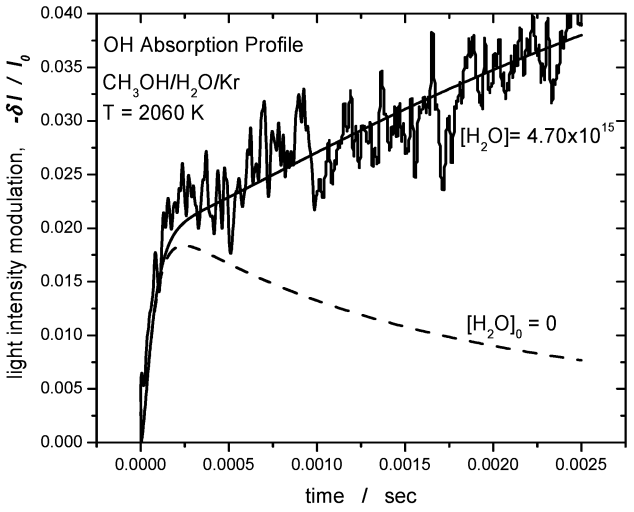

Figure 7. Sample OH profile in an experiment with water addition. The thin line with noise is an experimental profile for OH absorption acquired with water added to the reaction mixture: [Kr] = 2.393×10^{18}, $[CH_3OH]_0 = 1.196 \times 10^{13}$, and $[H_2O] = 4.703 \times 10^{15}$ molecule cm^{-3} at $T = 2060$ K. The solid line is a prediction of the mechanism for these experimental conditions, and the dashed line is a prediction of the mechanism for the same reaction mixture with no water added.

at 1 atm. Dombrowsky et al.[28] have experimentally measured branching ratios using both OH optical absorption and H-atom atomic resonance absorption spectroscopy (ARAS). From OH measurements, the reported branching ratio for reaction 3a was 80 ± 8%. From ARAS experiments, the branching ratio for reaction 3c was ≤ 5% with the other processes, reactions 3b and 3d−3f, giving ≤ 15%. Hence, these results do not agree with the theory presented by Xia et al.[3]

The present branching ratio results on the thermal decomposition of CH_3OH can be easily summarized. Using 16 of the experiments given in Table 1, we obtain a branching ratio for reaction 3a, $\alpha_{3a} = 0.94 \pm 0.09$, in agreement with Dombrowsky et al.[28] within combined experimental error.

Experiments with H_2O Addition. Both major routes for OH consumption in our experiments, reaction 1b and the self-reaction, produce water as a product. These major consumption channels can be completely repressed by shifting the equilibria in these reactions toward the reactants by the addition of water to the reaction mixture; that is, by dramatically increasing the rates for the back reactions. OH profiles obtained under such conditions represent an additional test for the validity of the reaction mechanism used in the data modeling.

Eighteen experiments were performed with $CH_3OH/H_2O/Kr$ mixtures over the temperature range 1683−2460 K with mole fractions of CH_3OH and H_2O of 1.4×10^{-5} and 2×10^{-3}, respectively. A sample profile is shown in Figure 7. The solid line in this graph is the model prediction for this mixture. After initial OH formation from CH_3OH decomposition, [OH] increases due to secondary reactions. Simulations indicate that [OH] can maximize in ∼ 5−10 ms up to 5 times $[CH_3OH]_0$, depending on temperature. The analysis shows that this increase is caused by several processes. First, methyl radicals react with water producing OH:

$$CH_3 + H_2O \rightarrow CH_4 + OH \quad (8)$$

Subsequently, methane decomposes producing additional methyl radicals and hydrogen atoms:

$$CH_4 \rightarrow CH_3 + H \quad (9)$$

Hydrogen atoms react with water producing hydroxyl radicals:

$$H + H_2O \rightarrow H_2 + OH \quad (10)$$

Essentially, CH_3 radicals catalyze the dissociation of H_2O through reactions 8 and 9. The direct reaction

$$H_2O \rightarrow H + OH \quad (11)$$

is too slow to produce significant amounts of OH on the time scale of the experiments. Due to the major role played by these processes in [OH] formation, no firm conclusions can be drawn concerning the relative roles of reactions 1a−1g from these experiments. However, the agreement between the modeled and experimental profiles confirms the validity of the mechanism (particularly the secondary reactions) used in the profile modeling.

Conclusions

Rate constants for reactions 1 and 2 and for the thermal decomposition of CH_3OH have been measured in this work. The values for (1) are the first determinations at temperatures > 1200 K, and the values for (2) appear to be the first ever reported. The implications for the OH + CH_3 reaction in combustion systems is straightforward. Based on the theoretical work of De A. Pereira et al.,[2] Xia et al.,[3] and Wilson and Balint-Kurti,[4] our analysis suggests that reactions 1b and 1g, for $T >$ ∼2000 K, give exclusively $H_2O + {}^1CH_2$ and ${}^3CH_2$ in a ratio of about two to one. In combustion systems under usual flame conditions, the ${}^1CH_2$ species will be instantaneously converted to ${}^3CH_2$, especially in the presence of O_2 where it is now known that intersystem crossing is the only important process with a rate constant for ${}^1CH_2 + O_2 \rightarrow {}^3CH_2 + O_2$ of $\sim 5 \times 10^{-11}$ cm^3 $molecule^{-1}$ s^{-1}.[29,30] Hence, we suggest that the present experimental result, eq E2, can be used to assess the rate for the overall process, OH + CH_3 = ${}^3CH_2$ + H_2O, for use in combustion modeling.

Acknowledgment. The authors wish to thank Drs. Jan P. Hessler and N. Srinivasan for valuable discussions and Dr. B. Ruscic for supplying a purified sample of ketene. This work was supported by the U. S. Department of Energy, Office of Basic Energy Sciences, Division of Chemical Sciences, Geosciences and Biosciences under Contract No. W-31-109-Eng-38.

Supporting Information Available: The complete mechanisms with rate constants, used for the simulations presented in the paper, are given as a supplementary table. This material is available free of charge via the Internet at http://pubs.acs.org.

References and Notes

(1) *NIST Chemical Kinetics Database*; NIST Standard Reference Database 17, Gaithersburg, MD, 2000.
(2) De A. Pereira, R.; Baulch, D. L.; Pilling, M. J.; Robertson, S. H.; Zeng, G. *J. Phys. Chem. A* **1997**, *101*, 9681.
(3) Xia, W. S.; Zhu, R. S.; Lin, M. C.; Mebel, A. M. *Faraday Discuss.* **2001**, *119*, 19.
(4) Wilson, C.; Balint-Kurti, G. G. *J. Phys. Chem. A* **1998**, *102*, 1625.
(5) Cribb, P. H.; Dove, J. E.; Yamazaki, S. *Combust. Flame* **1992**, *88*, 169.
(6) Krasnoperov, L. N.; Michael, J. V. *J. Phys. Chem. A* **2004**, *108*, 5643.
(7) Michael, J. V. *Prog. Energy Combust. Sci.* **1992**, *18*, 327.
(8) Michael, J. V. In *Advances in Chemical Kinetics and Dynamics*; Barker, J. R., Ed.; JAI: Greenwich, 1992; Vol. I, pp 47−112, for original references.

(9) Michael, J. V.; Sutherland, J. W. *Int. J. Chem. Kinet.* **1986**, *18*, 409.

(10) Michael, J. V. *J. Chem. Phys.* **1989**, *90*, 189.

(11) Michael, J. V.; Fisher, J. R. In *Seventeenth International Symposium on Shock Waves and Shock Tubes*, AIP Conference Proceedings 208; Kim, Y. W., Ed.; American Institute of Physics: New York, 1990; pp 210−215.

(12) Su, M.-C.; Kumaran, S. S.; Lim, K. P.; Michael, J. V. *Rev. Sci. Instrum.* **1995**, *66*, 4649.

(13) Su, M.-C.; Kumaran, S. S.; Lim, K. P.; Michael, J. V.; Wagner, A. F.; Harding, L. B.; Fang, D.-C. *J. Phys. Chem. A* **2002**, *106*, 8261.

(14) Grebenkin, S. Yu.; Krasnoperov, L. N. *J. Phys. Chem. A* **2004**, *108*, 1953.

(15) Bott, J. F.; Cohen, N. *Int. J. Chem. Kinet.* **1989**, *21*, 485.

(16) (a) Walter, D.; Grotheer, H.-H.; Davies, J. W.; Pilling, M. J.; Wagner, A. F. *Proc. Combust. Inst.* **1990**, *23*, 107. (b) Hwang, S. M.; Rabinowitz, M. J.; Gardiner, W. C., Jr. *Chem. Phys. Lett.* **1993**, *205*, 157. (c) Davidson, D. F.; Di Rosa, M. D.; Chang, A. Y.; Hanson, R. K.; Bowman, C. T. *Proc. Combust. Inst.* **1992**, *24*, 589. (d) Davidson, D. F.; Hanson, R. K.; Bowman, C. T. *Int. J. Chem. Kinet.* **1995**, *27*, 305.

(17) Wooldridge, M. S.; Hanson, R. K.; Bowman, C. T. *Int. J. Chem. Kinet.* **1994**, *26*, 389.

(18) Hochanadel, C, J.; Sworski, T. J.; Ogren, P. J. *J. Phys. Chem.* **1980**, *84*, 129.

(19) Anastasi, C.; Ellermann, P.; Pagsberg, P.; Polak, S. *J. Chem. Soc., Faraday Trans.* **1991**, *87*, 2991.

(20) Fagerstrom, K.; Lund, A.; Mahmoud, G.; Jadkowski, J. T.; Ratajczak, E. *Chem. Phys. Lett.* **1993**, *206*, 226.

(21) Laszlo, B.; Dobe, S.; Berces, T.; Marta, F. *Twelfth International Symposium on Gas Kinetics*; 1992.

(22) Oser, H.; Stothard, N. D.; Humpfer, R.; Grotheer, H.-H.; Just, Th. *Proc. Combust. Inst.* **1992**, *24*, 597. Humpfer, R.; Oser, H.; Grotheer, H.-H.; Just, Th. *Proc. Combust. Inst.* **1994**, *25*, 721. Humpfer, R.; Oser, H.; Grotheer, H.-H. *Int. J. Chem. Kinet.* **1995**, *27*, 577.

(23) Hughes, K. J.; Pereira, R. A.; Pilling, M. J. *Ber. Bunsen−Ges. Phys. Chem.* **1992**, *92*, 1352.

(24) Bott, J. F.; Cohen, N. *Int. J. Chem. Kinet.* **1991**, *23*, 1017.

(25) Tsang, W.; Hampson, R. F. *J. Phys. Chem. Ref. Data* **1986**, *15*, 1087.

(26) Frank, P.; Bhaskaran, K. A.; Just, Th. *J. Phys. Chem.* **1986**, *90*, 2226.

(27) Baulch, D. L.; Cobos, C. J.; Cox, R. A.; Frank, P.; Hayman, G.; Just, Th.; Kerr, J. A.; Murrells, T.; Pilling, M. J.; Troe, J.; Walker, R. W.; Warnatz, J. *J. Phys. Chem. Ref. Data* **1994**, *23*, 411.

(28) Dombrowsky, Ch.; Hoffman, A.; Klatt, M.; Wagner, H. Gg. *Ber. Bunsen−Ges. Phys. Chem.* **1991**, *95*, 1685.

(29) Hancock, G.; Haverd, V. *Chem. Phys. Lett.* **2003**, *372*, 288.

(30) Blitz, M. A.; McKee, K. W.; Pilling, M. J.; Seakins, P. W. *Chem. Phys. Lett.* **2003**, *372*, 295.